Electronic Supplementary Information for

Synthesis, Characterization, and High-Pressure Studies of a 3D Berkelium(III) Carboxylate Framework Material

Joseph M. Sperling,[a] Nicholas Beck,[a] Benjamin Scheibe,[a] Zhuanling Bai,[a] Jacob Brannon,[a] Daniela Gomez Martinez,[a] Dennis Grödler,[b] Jason A. Johnson,[c] Xinsong Lin,[a] Brian M. Rotermund,[a] and Thomas E. Albrecht-Schönzart[a]*

[a]Department of Chemistry and Biochemistry, Florida State University, 95 Chieftan Way, RM. 118 DLC, Tallahassee, Florida 32306, USA

[b]Department of Chemistry, Institute for Inorganic Chemistry, University of Cologne, Greinstr. 4-6, 50939 Cologne Germany

[c]Environmental Health and Safety, Florida State University, Tallahassee, Florida 32310, USA

Table of Contents

Experimental Details.

General Precautions:

CAUTION!!!!! *Berkelium-249 ($t_{1/2}$ = 0.9 years; specific activity = 6.1 × 10^{10}Bq/mg) is a very serious internal health hazard from its β-emission of 123 keV. Berkelium-249 decays the majority of the time (99.99855% probability) to californium-249 which is a serious internal health hazard from high energy (5.813 MeV; 82.2% branch) α-radiation and is also a serious external health hazard owing to its high energy (388 keV; 66% branch) γ-radiation. All handling of radioactive material was choreographed with non-radioactive material and operational procedures were approved by radiation safety prior to any experiments involving radioactive material. All handling of radioactive material was completed in a Category II radiological facility and all workers wore appropriate protective equipment while handling radioactive material. Due to the short half-life of berkelium-249, the californium-249 daughter has an in-growth of 1.5% per week. The experiments that took place below were all completed 34 days after the most recent berkelium/californium separation completed at Oak Ridge National Lab (ORNL). This brings the californium content to a 6.84% impurity based on the appropriate Bateman Equation*.

Materials:

Mellitic acid ($C_6(COOH)_6$ 99%, Sigma-Aldrich), $HBr_{(aq)}$ (48%, Sigma-Aldrich), DI H_2O (18 MΩ), ethanol (EtOH, Absolute, Koptek), diethyl ether (99%, Fisher Scientific) were all used as received. The ^{249}Bk was supplied by the Radiochemical Engineering Development Center (REDC) at ORNL.

Synthesis:

$Bk_2[C_6(CO_2)_6](H_2O)_8 \cdot 2H_2O$ (Bk1): Freshly precipitated berkelium hydroxide (*ca.* 3.5 mg, 0.014 mmol Bk content) was dissolved in an excess of HBr (~ 1mL, 48%, 8.77 M) and transferred to a 20 mL scintillation vial. The aqueous berkelium solution was evaporated to dryness forming a hydrated $BkBr_3$ residue using a heat lamp and a slow stream of nitrogen. The $BkBr_3 \cdot nH_2O$ residue was washed with diethyl ether (2 × 1 mL) to dissolve and remove imbedded Br_2 formed from the oxidation of HBr. The hydrated residue was dissolved in DI H_2O (0.5 mL) and the solution was transferred to a 7 mL scintillation vial. An aqueous solution of excess mellitic acid (23.9 mg, 0.07 mmol) dissolved in DI H_2O (0.3 mL) was added dropwise to the berkelium solution. Ethanol (4 mL) was then slowly layered on top of the aqueous berkelium mellitate solution. After three hours, a small crop of crystals was formed. The 7 mL vial was slowly tilted so that the crystals would concentrate at the bottom corner of the vial. The supernatant was then transferred to a 20 mL scintillation vial. The crystals were then washed with ethanol (1 × 1 mL) to facilitate isolating the crystals with a copper spatula and immersion oil.

Single crystal X-ray diffraction:

Crystals of **Bk1** were selected under immersion oil and mounted on a MiTeGen MicroLoop. Intensity data of a suitable crystal were recorded at 100 K with an XtaLAB Synergy-S diffractometer (Rigaku) equipped with a Cryostream 800 (Oxford Cryosystems). The diffractometer was operated with monochromatized Mo-K_α radiation (0.71073 Å, multi-layered optics) and equipped with a HyPix-6000HE detector. Evaluation, integration, and reduction of the diffraction data were carried out with the CrysAlis Pro software suite.[1] The diffraction data were corrected for absorption utilizing both the multi-scan and spherical method within the CrysAlis Pro software suite. The structure was solved with dual-space methods (SHELXT) and refined against F^2 with SHELXL in the Olex2 software suite.[2-4] All non-hydrogen atoms were refined with anisotropic displacement parameters, all hydrogen atoms were located from the difference map and refined with isotropic displacement parameters. CCDC 2125963 contains the supplementary crystallographic data for this paper. These data are provided free of charge by The Cambridge Crystallographic Data Centre. We don't expect that the estimated Cf content of ~7% significantly alters the determined Bk – O bond lengths since the comparison of the isotypic Bk – O and Cm – O bond lengths are usually the same within the tripled standard uncertainties. Therefore, the daughter was not taken into account during structural refinement. Furthermore, the

known Cf mellitate crystallizes in a different structure type with a coordination number of eight for the Cf atom instead of nine and can therefore not be used in comparison.

Solid-State UV-vis-NIR Absorption Spectroscopy:

Crystals of **Bk1** under immersion oil on a glass slide were placed on the stage of a Craic Technologies 20/20 PV dual microspectrophotometer. 100 W Hg and 75 W Xe lamps were used for photoluminescence and transmission, respectively. Integration times were optimized by using the Craic Technologies software. For low temperature absorption spectroscopy, 8 crystals were selected and transferred to a quartz slide and placed in a Linkam LTS420 temperature controlled stage placed on the Craic microspectrophotometer. The stage was purged for 5 minutes with nitrogen and then cooled at 5 °C/min to −180 °C. Spectra were then measured by optimizing the integration times using the Craic Software. It is important to note that the broad feature in the high energy region of the spectrum (Fig. S9-S10) from 27,000 – 30,000 cm^{-1} (320 – 370 nm) is caused by detector saturation and cannot be undoubtedly attributed to a real transition.

Variable Pressure Absorption Spectroscopy:

A steel gasket with 200 μm thickness was indented to around 70 μm and a 150 μm diameter hole was drilled through the center with a Boehler μDriller electric drill. The gasket was placed on a diamond with a 500 μm culet in a DACTools SSDAC80. A single crystal of **Bk1** was placed in the gasket hole along with a few ruby spheres. Polydimethylsiloxane was added for the pressure medium. Pressure was controlled *via* a pressure membrane and a gas pressure controller using helium gas. Pressure was monitored by measuring the fluorescence of the ruby[5] around 694 nm excited by a 532 nm laser on the Craic Technologies 20/20 PV dual microspectrophotometer. Absorption was measured at each pressure using the microspectrophotometer. After the highest pressure was achieved, the pressure was released and the cell was opened and absorption was re-measured at ambient pressures.

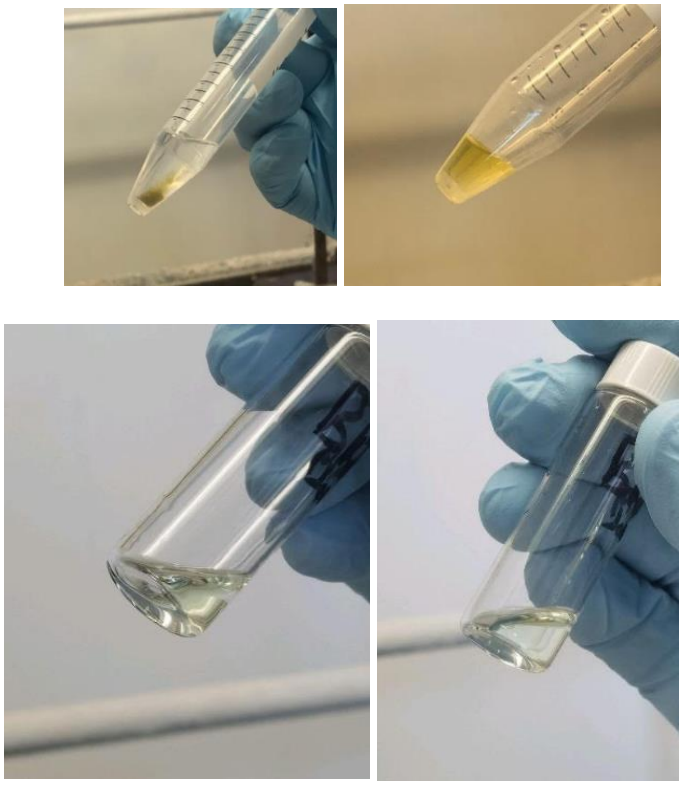

Figure S2. $Bk^{3+}_{(aq)}$ solution before (left) and after the addition of mellitic acid (right).

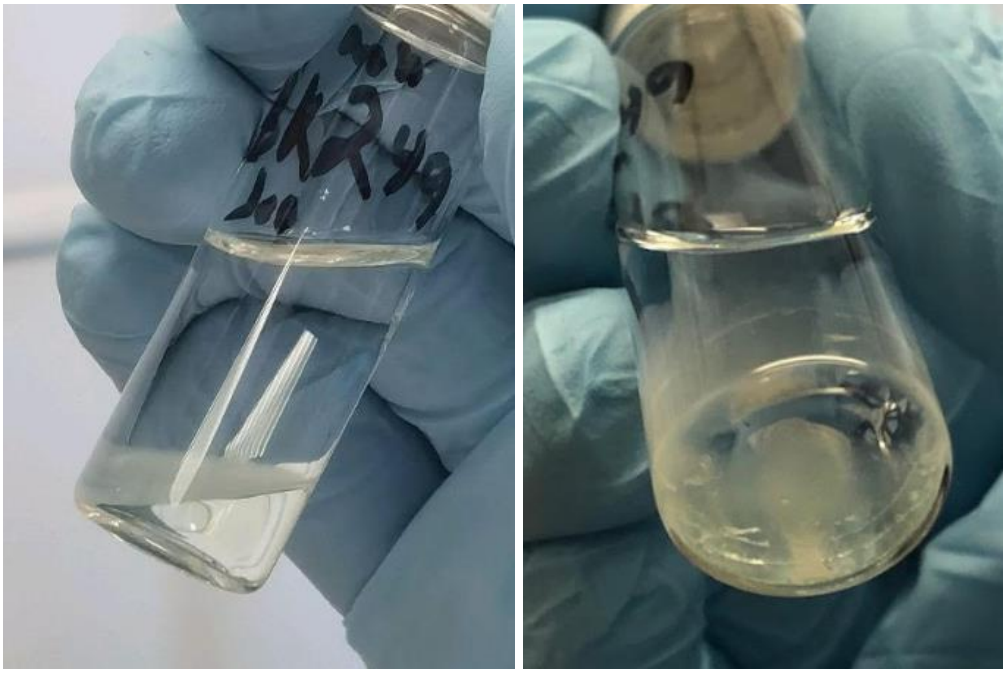

Figure S3. Layered berkelium mellitate solutions just after ethanol layering (left) and three hours later (right).

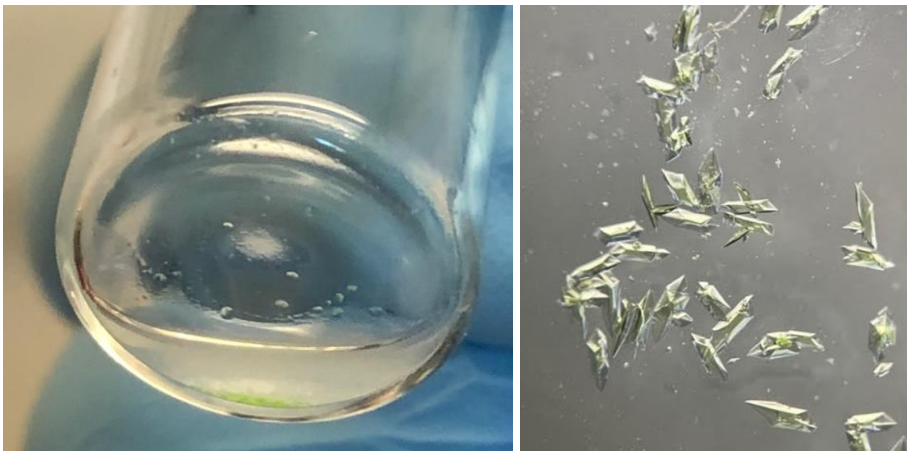

Figure S4. Bulk sample of **Bk1** (left) and crystals of **Bk1** under a microscope (right).

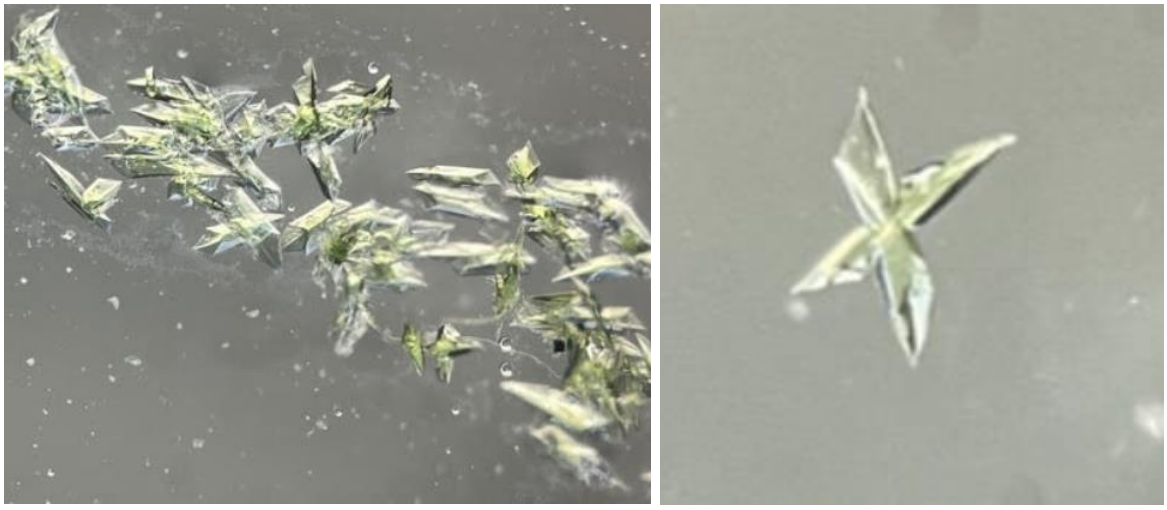

Figure S5. Crystals of **Bk1** under a microscope.

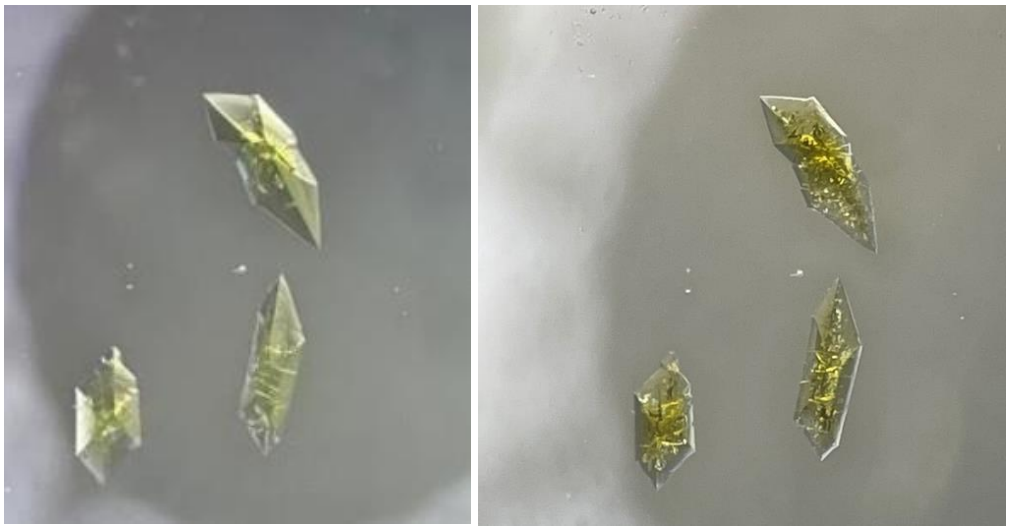

Figure S6. Crystals of **Bk1** 14 days after (left) and 28 days after (right) initial synthesis.

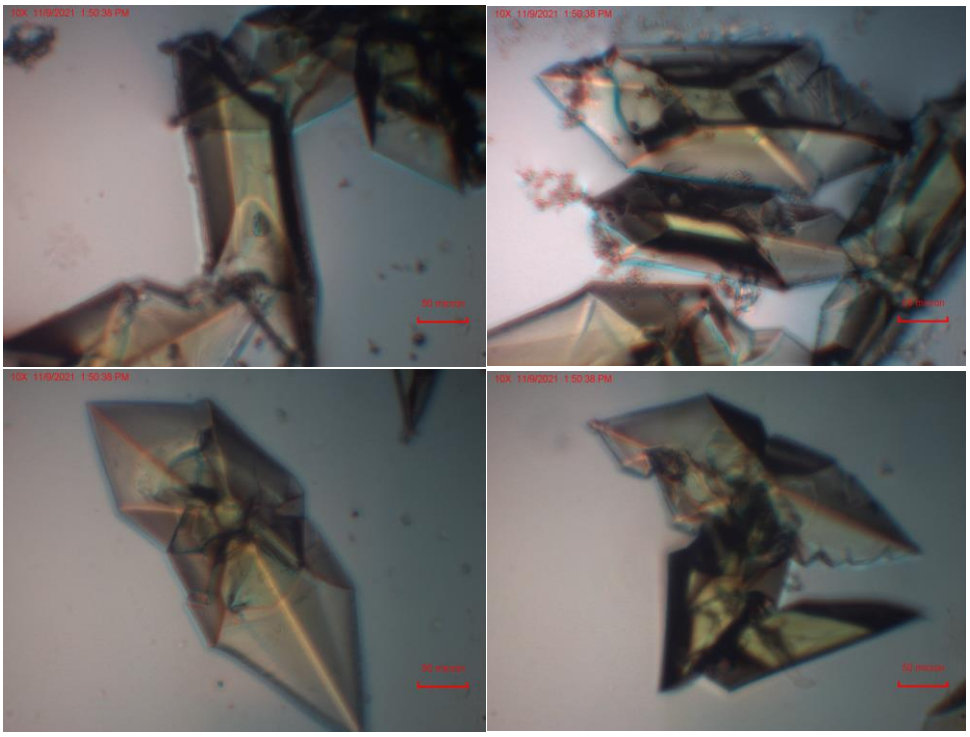

Figure S7. Crystals of **Bk1** under the microscope of the microspectrophotometer.

Supplementary Crystallographic Information:

Table S1. Selected crystallographic data and details of the structure determination of **Bk1.**

Formula	$Bk_1C_6O_{11}H_{10}$
Molar mass / g·mol^{-1}	507.22
Space group (No.)	*P* 1 2_1/*n* 1 (14)
***a* / Å**	8.4703(2)
b	13.0851(3)
***c* / Å**	9.5474(2)
***β* / °**	96.023(2)
***V* / Å^3**	1052.34(4)
Z	4
Pearson code	*mP*72 (without H atoms)
$\rho_{calc.}$ / g·cm^{-3}	3.201
μ / mm^{-1}	7.805
Color	pale green
Crystal habitus	block
Crystal size / mm^3	0.06 × 0.09 × 0.19
***T* / K**	100
λ / Å	0.71073 (Mo-K_α)
No. of reflections	15900
ϑ range / °	3.40-30.52
Range of Miller indices	$-12 \le h \le 11$
	$-18 \le k \le 18$
	$-13 \le l \le 13$
Absorption correction	multi-scan
T_{max}, T_{min}	0.580, 0.572
R_{int}, R_σ	0.0210, 0.0144
Completeness of the data set	0.988
No. of unique reflections	3174
No. of parameters	204
No. of restraints	0
No. of constraints	0
***S* (all data)**	1.156
***R*(*F*) (*I* ≥ 2σ(*I*), all data)**	0.0133, 0.0142
***wR*(F^2) (*I* ≥ 2σ(*I*), all data)**	0.0292, 0.0294
Extinction coefficient	0.00070(5)
$\Delta\rho_{max}$, $\Delta\rho_{min}$ / e·Å^{-3}	0.910, −0.892

Table S2. Atomic distances for **Bk1**.

Atom	Atom	Length/Å	Atom	Atom	Length/Å
Bk1	O1	2.5148(17)	O3	C1	1.260(3)
Bk1	O4	2.5730(17)	O2	C3	1.264(3)
Bk1	O3	2.5446(16)	O1B	C2	1.247(3)
Bk1	O3W	2.4654(18)	O2B	C2	1.259(3)
Bk1	O4W	2.4811(18)	C1	C4	1.506(3)
Bk1	O2W	2.4454(18)	C3	C6	1.500(3)
Bk1	O2	2.5212(17)	C6	C4	1.400(3)
Bk1	O1W	2.3739(18)	C6	C5	1.405(3)
Bk1	O1B	2.3552(16)	C2	C5	1.526(3)
Bk1	C1	2.932(2)	C4	C5	1.398(3)
Bk1	C3	2.886(2)	O1	C3	1.261(3)
Bk1	C2	3.601(2)	O4	C1	1.278(3)

Table S3. Comparative bond lengths (in Å) with isostructural actinide mellitates, $An_2[C_6(CO_2)_6](H_2O)_8{\cdot}2H_2O$.

	Puβ[6]	Am[7]	Cm[8]	Bk
M – O1	2.543(3)	2.543(3)	2.530(3)	2.5148(17)
M – O2	2.561(3)	2.546(3)	2.534(3)	2.5212(17)
M – O3	2.581(2)	2.577(2)	2.567(3)	2.5446(16)
M – O4	2.591(3)	2.591(3)	2.581(3)	2.5730(17)
M – O1B	2.389(2)	2.375(3)	2.364(3)	2.3552(16)
M – O1W	2.426(3)	2.415(3)	2.397(3)	2.3739(18)
M – O2W	2.494(3)	2.484(3)	2.465(3)	2.4454(18)
M – O3W	2.520(3)	2.501(3)	2.484(3)	2.4654(18)
M – O4W	2.529(3)	2.516(3)	2.496(3)	2.4811(18)

Table S4. Bond Angles for Bk1.

Atom	Atom	Atom	Angle/˚	Atom	Atom	Atom	Angle/˚
O1	Bk1	O4	112.91(5)	O1B	Bk1	O1	123.51(6)
O1	Bk1	O3	68.04(5)	O1B	Bk1	O4	121.32(6)
O1	Bk1	O2	51.73(5)	O1B	Bk1	O3	141.27(6)
O3W	Bk1	O1	72.87(6)	O1B	Bk1	O3W	136.69(6)
O3W	Bk1	O4	72.43(6)	O1B	Bk1	O4W	70.08(6)
O3W	Bk1	O3	80.96(6)	O1B	Bk1	O2W	78.86(6)
O3W	Bk1	O4W	149.48(6)	O1B	Bk1	O2	76.48(6)
O3W	Bk1	O2	122.50(6)	O1B	Bk1	O1W	68.11(6)
O4W	Bk1	O1	106.59(6)	O2W	Bk1	O2	75.78(6)
O4W	Bk1	O4	80.34(6)	O2	Bk1	O4	138.54(6)
O4W	Bk1	O3	71.19(6)	O2	Bk1	O3	90.63(6)
O4W	Bk1	O2	71.13(6)	O1W	Bk1	O1	148.98(6)
O2W	Bk1	O1	68.93(6)	O1W	Bk1	O4	72.22(6)
O2W	Bk1	O4	140.35(6)	O1W	Bk1	O3	123.33(6)
O2W	Bk1	O3	133.65(6)	O1W	Bk1	O3W	80.40(6)
O2W	Bk1	O3W	70.67(6)	O1W	Bk1	O4W	104.43(6)
O2W	Bk1	O4W	138.74(6)	O1W	Bk1	O2W	87.74(7)
O1W	Bk1	O2	143.23(6)				

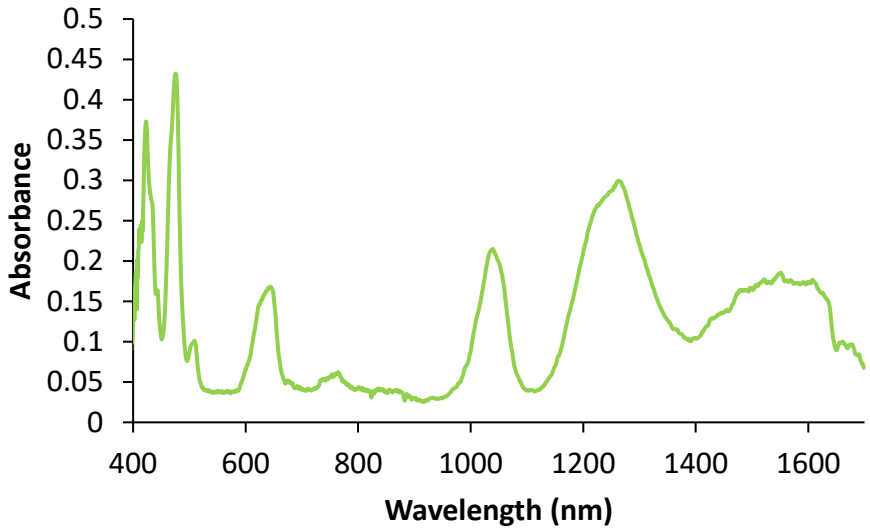

Figure S8. Solid-state UV-vis-NIR spectrum of **Bk1** at room temperature and ambient pressure plotted in nanometers.

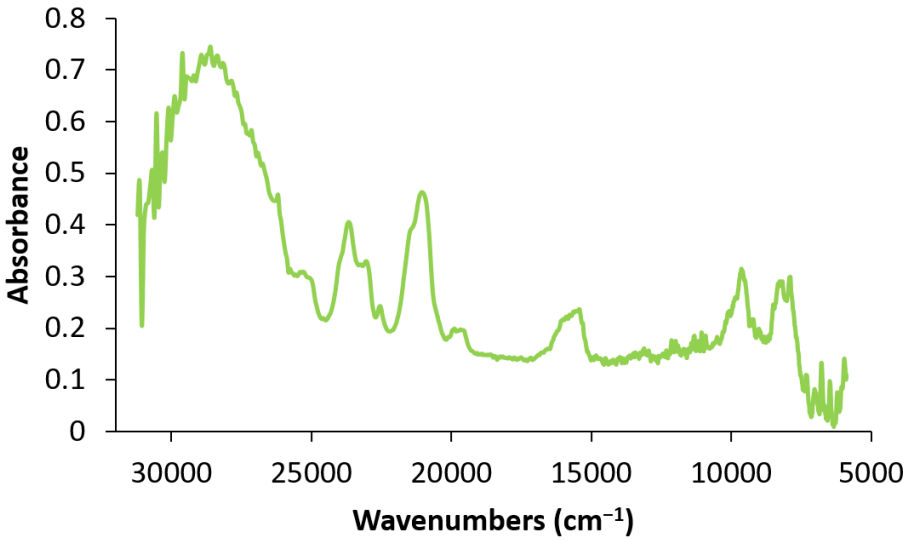

Figure S9. Solid-state UV-vis-NIR spectrum of **Bk1** at −180 °C and ambient pressure plotted in wavenumbers.

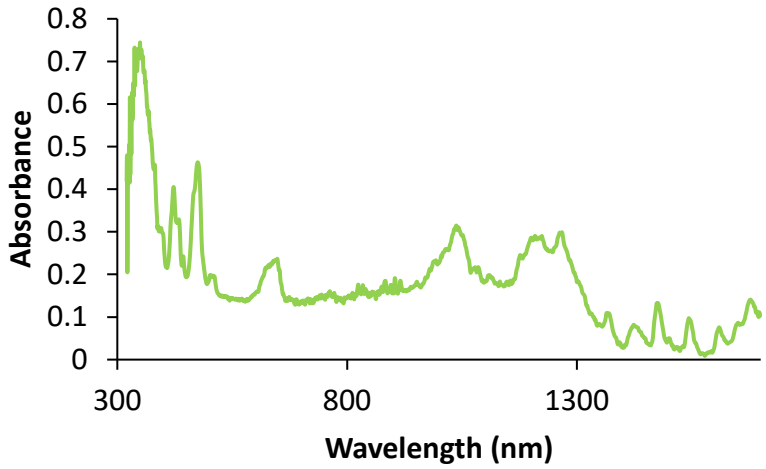

Figure S10. Solid-state UV-vis-NIR spectrum of **Bk1** at −180 °C under ambient pressure plotted in nanometers

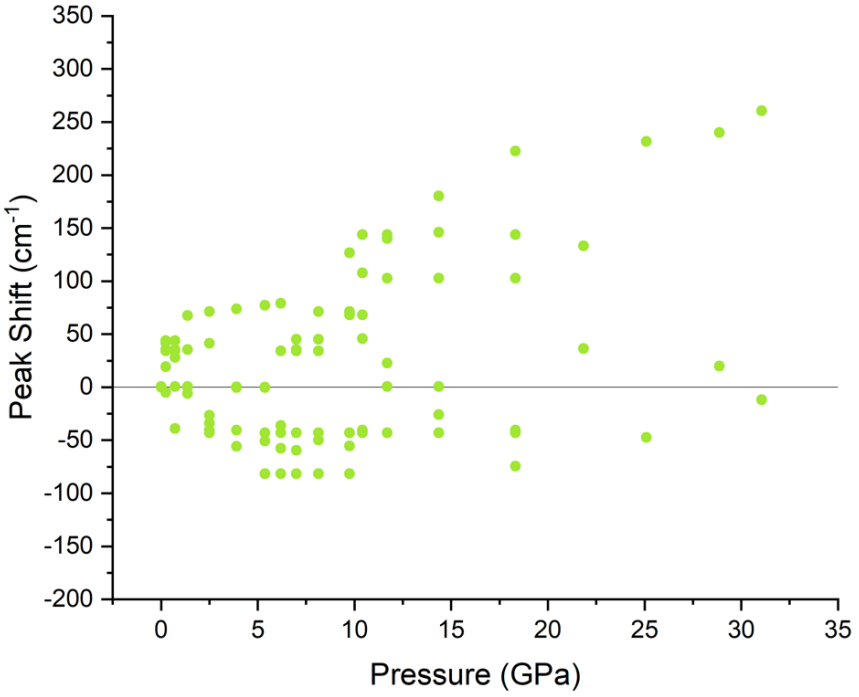

Figure S11. Peak shifts of several transitions relative to ambient pressure of **Bk1** as a function of pressure at room temperature.

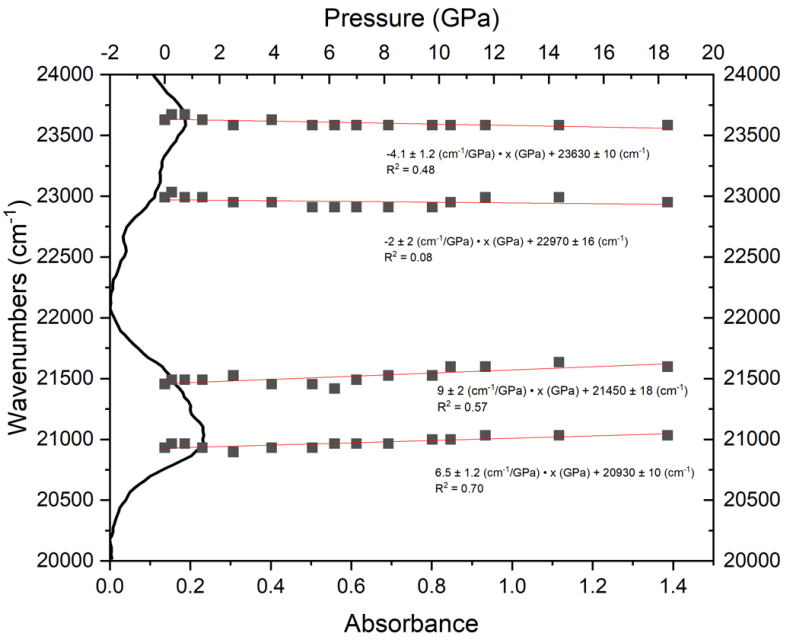

Figure S12. The solid-state absorption spectrum of **Bk1** focusing on the Group E and F transitions plotted along the *y*-axis at ambient pressure, with their peak positions plotted as a function of pressure.

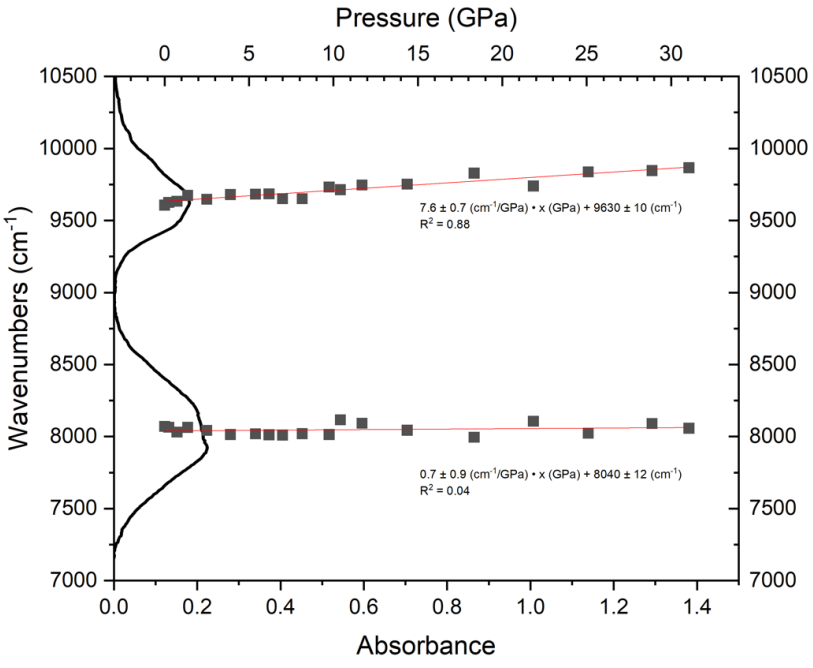

Figure S13. The solid-state absorption spectrum of **Bk1** focusing on the Group A and B transitions plotted along the *y*-axis at ambient pressure with their peak positions plotted as a function of pressure.

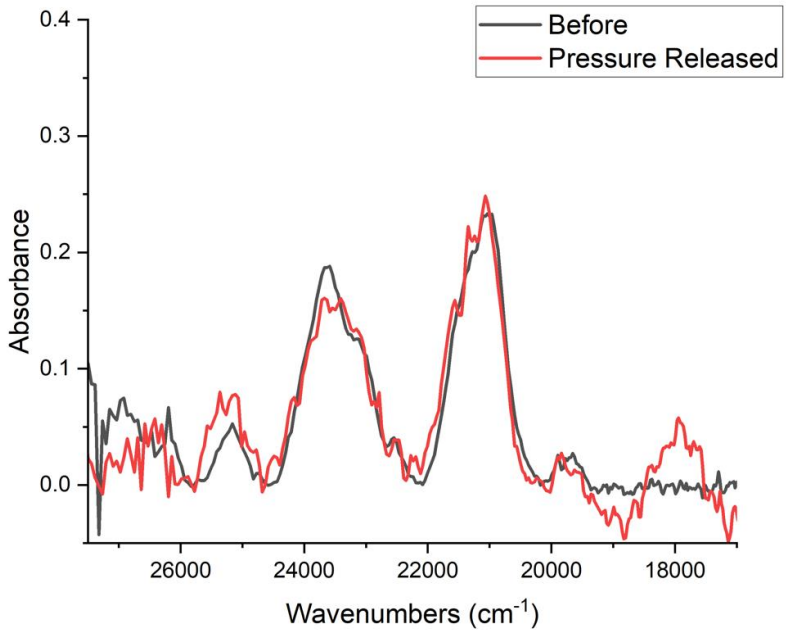

Figure S14. Solid-state absorption spectra of **Bk1** before pressure was applied and after the maximum pressure of 31.06 GPa released.

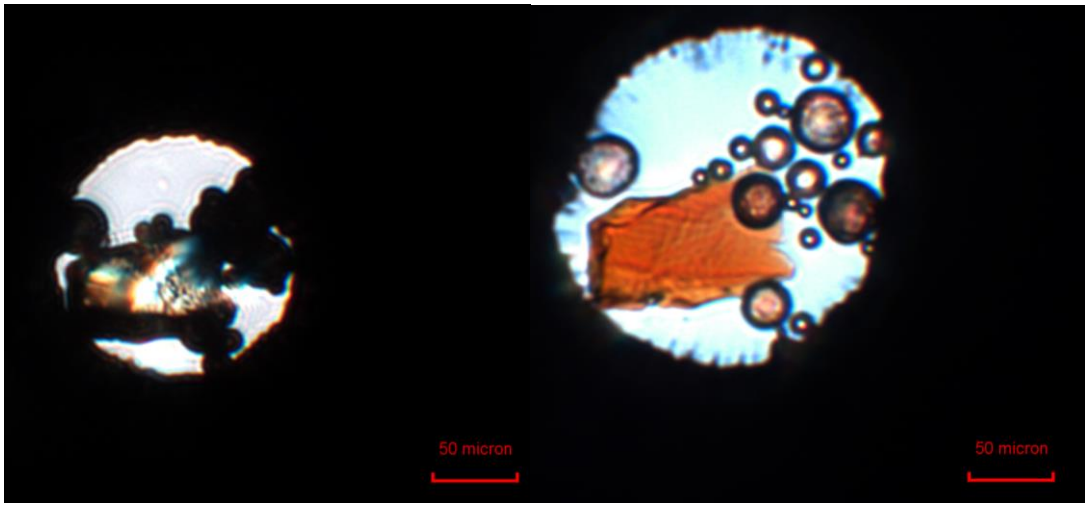

Figure S15. Crystal of **Bk1** inside the diamond anvil cell slightly above ambient pressure (left) and at 31.06 GPa (right). Small spherical ruby crystals are also visible.

References

1. *CrysAlisPro, Version 1.171.41.115a*, Rigaku Oxford Diffraction, Oxford, UK, 2021.
2. G. M. Sheldrick, *Acta Crystallogr., Sect. A: Found. Adv.* 2015, ***71***, 3-8.
3. G. M. Sheldrick, *Acta Crystallogr., Sect. C: Struct. Chem.* 2015, ***71***, 308.
4. O. V. Dolomanov, L. J. Bourhis, R. J. Gildea, J. A. K. Howard, H. Puschmann, *J. Appl. Crystallogr.* 2009, ***42***, 339-341.
5. A. D. Chijioke, W. Nellis, A. Soldatov, I. F. Silvera, *J. Appl. Phys.* 2005, ***98***, 114905.
6. J. M. Sperling, A. N. Gaiser, C. J. Windorff, B. E. Klamm, M. A. Whitefoot, A. T. Chemey, B. N. Long, J. G. Campbell, T. E. Albrecht-Schmitt, *Inorg. Chem.* 2020, ***59***, 3085-3090.
7. J. M. Sperling, E. J. Warzecha, C. Celis-Barros, D.-C. Sergentu, X. Wang, B. E. Klamm, C. J. Windorff, A. N. Gaiser, F. D. White, D. A. Beery, A. T. Chemey, M. A. Whitefoot, B. N. Long, K. Hanson, P Kögerler, M. Speldrich, E. Zurek, J. Autschbach, and T. E. Albrecht-Schönzart, *Nature*, 2020, ***583***, 396-399.
8. J. M. Sperling, E. Warzecha, B. E. Klamm, A. N. Gaiser, C. J. Windorff, M. A. Whitefoot, T. E. Albrecht-Schönzart, *Inorg. Chem.* 2021, ***60***, 476-483.